Nonlinear simulation of toroidal Alfvén eigenmodes in the presence of a tearing mode

J. Zhu, Z. W. Ma[(a)], S. Wang, and W. Zhang

Institute for Fusion Theory and Simulation,

Zhejiang University, Hangzhou, Zhejiang 310027, China

Abstract

A hybrid simulation is carried out to study nonlinear dynamics of $n = 1$ toroidal Alfvén eigenmodes (TAEs) with the $m/n = 2/1$ tearing mode. It is found that the $n = 1$ TAE is first excited by isotropic energetic particles at the linear stage and reaches the first steady state due to wave-particle interaction. After the saturation of the $n = 1$ TAE, the m/n=2/1 tearing mode grows continuously and reaches its steady state due to nonlinear mode-mode coupling, especially, the $n = 0$ component plays a very important role in the tearing mode saturation. The results suggest that the enhancement of the tearing mode activity with increase of the resistivity could weaken the TAE frequency chirping through the interaction between the $p = 1$ TAE resonance and the $p = 2$ tearing mode resonance for passing particles in the phase space, which is opposite to the classical physical picture of the TAE frequency chirping that is enhanced with dissipation increase.

[a)]Author to whom correspondence should be addressed: zwma@zju.edu.cn

I. INTRODUCTION

Tearing mode instability is a ubiquitous phenomenon in space and laboratory plasmas. Tearing mode can cause the topological change of magnetic field lines and convert magnetic energy into plasma kinetic energy. In tokamak experiments, tearing modes will degrade confinement and determine the successful operation of burning plasma experiments.

In burning plasmas, the interaction between Alfvén waves and energetic particles that come from nuclear fusion products or auxiliary heating is one of important issues in current and future magnetic confinement fusion researches[1]. Toroidicity-induced discrete shear Alfvén eigenmode (TAE)[2, 3] can exist with its frequencies inside the gaps of the Alfvén continuum spectra in toroidal plasmas.

The nonlinear mode couplings between shear Alfvén waves and magnetic islands (due to tearing mode instability) are observed in tokamak experiments, such as HL-2A[4–6] and J-TEXT[7]. The axis-symmetry magnetic activities with $n = 0$ have been observed during neutral beam injection (NBI) on HL-2A and interpreted that these modes are generated by the nonlinear mode coupling via the decay process between high frequency Alfvén eigenmodes and low-frequency magnetohydrodynamics (MHD) modes[4]. Besides, for the strong AE mode and TM mode coupling case, TAEs show a weak chirping feature while pitch-fork TAEs are observed associated with weak tearing mode activities[5].

Effects of energetic particles on the internal kink mode and Alfvén eigenmodes have been studied extensively. The energetic particle stabilization on the internal kink mode has been investigated analytically and numerically[8]. The stabilization is associated with conservation of the third invariant when the energetic particle precession frequency is much larger than the MHD growth rate. TAEs can be driven by energetic particles (EPs) through wave-particle interaction[9, 10]. EP transport and loss associated with TAEs have attracted a lot of attention recently. However, investigations in energy particle effects on linear and nonlinear dynamics of a tearing mode stability are limited. The first simulation in energetic particle effects on the $m/n = 2/1$ tearing mode in the tokamak geometry was carried out with the NIMROD code by Takahashi[11] et. al. They found that energetic particles have damping and stabilizing effects on $m/n = 2/1$ tearing mode. The theoretical work was

done by Cai et. al[12] to investigate the influence of circulating energetic ions (CEI) on tearing modes. It was found that the effects of CEI on tearing modes mainly depend on the toroidal circulating direction: tearing modes could be stabilized by co-CEI while the growth of tearing modes is enhanced by counter-CEI. The related simulation work to validate their analytical results is also carried out using hybrid code M3D-K[13]. Previous study is mainly on energy particle effects on the linear stability of the tearing mode and it is still a lack of reports in the interaction between tearing modes and TAEs driven by energy particles.

In this paper, we use a hybrid kinetic-MHD code (CLT-K)[14] to study dynamics of the $m/n = 2/1$ tearing mode and the $n = 1$ TAE driven by isotropic energetic particles. The framework of the MHD part is based on the CLT code[15], which is a MHD code with three dimensional toroidal geometries. This paper is organized as follows. In Sec. II, the simulation model and numerical method are introduced. Then, our simulation results are presented In Sec. III. Finally, conclusion and discussion are given in Sec. IV.

II. SIMULATION MODEL

A. A brief review of CLT

The CLT code is an initial value code that solves the full set of resistive MHD equations in toroidal geometries:

$$\frac{\partial \rho}{\partial t} = -\nabla \cdot (\rho \mathbf{v}) + \nabla \cdot [D \nabla (\rho - \rho_0)], \tag{1}$$

$$\frac{\partial p}{\partial t} = -\mathbf{v} \cdot \nabla p - \Gamma p \nabla \cdot \mathbf{v} + \nabla \cdot [\kappa \nabla (p - p_0)], \tag{2}$$

$$\frac{\partial \mathbf{v}}{\partial t} = -\mathbf{v} \cdot \nabla \mathbf{v} + [\mathbf{J} \times \mathbf{B} - \nabla p]/\rho + \nabla \cdot [\nu \nabla (\mathbf{v} - \mathbf{v}_0)], \tag{3}$$

$$\frac{\partial \mathbf{B}}{\partial t} = -\nabla \times \mathbf{E}, \tag{4}$$

$$\mathbf{E} = -\mathbf{v} \times \mathbf{B} + \eta (\mathbf{J} - \mathbf{J}_0), \tag{5}$$

$$\mathbf{J} = \frac{1}{\mu_0} \nabla \times \mathbf{B}, \tag{6}$$

where the subscript of "0" represents equilibrium variables. Equations (1)-(6) are evolved in a cylindrical coordinate system (R, ϕ, Z). A finite difference method is employed in the R and Z directions with 4th order accuracy, while in the ϕ direction, either a finite difference or

pseudo-spectrum method is used. In the time-advance, the 4th order Runge-Kutta scheme is chosen.

B. The hybrid kinetic-MHD model

According to the current coupling formalism of the hybrid kinetic-MHD model[16], only one modification on the usual MHD equations is an additional energetic ion current $\mathbf{J}_h$ on the momentum equation:

$$\frac{\partial \mathbf{v}_b}{\partial t} = -\mathbf{v}_b \cdot \nabla \mathbf{v}_b + [(\mathbf{J} - \mathbf{J}_h) \times \mathbf{B} - \nabla p_b]/\rho_b + \nabla \cdot [\nu \nabla (\mathbf{v}_b - \mathbf{v}_{b0})], \tag{7}$$

where the subscripts "h" and "b" are adopted to distinguish between hot particles and bulk plasma. It should be noted that $Z_h e\mathbf{E}$ does not appear in the above momentum equation because of cancellation between $Z_h e\mathbf{E}$ and energetic particle $\mathbf{E} \times \mathbf{B}$ current. The approximation of this hybrid model is under the condition that the density of hot particle is much less than the bulk plasma density: $n_h \ll n_b$.

C. Equation of motion

We use the five-dimensional guiding-center equations of motion derived from the Northrop guiding-center Lagrangian in the presence of the $\mathbf{E} \times \mathbf{B}$ drift velocity[17] to push particles in the phase space:

$$\frac{d\mathbf{X}}{dt} = \frac{1}{B_{||}^*} \left[v_{||} \mathbf{B}^* + \mathbf{E}^* \times \mathbf{b} \right], \tag{8}$$

$$\frac{dv_{||}}{dt} = \frac{Z_h e}{m B_{||}^*} \mathbf{B}^* \cdot \mathbf{E}^*, \tag{9}$$

where the modified fields $\mathbf{B}^* = \nabla \times \mathbf{A}^*$ (with $B_{\|}^* \equiv \mathbf{B}^* \cdot \mathbf{b}$ and $\mathbf{b}$ is a unit vector of the magnetic field) and $\mathbf{E}^* = -\nabla \Phi^* - \partial \mathbf{A}^* / \partial t$ are expressed in terms of the new effective electric potential and vector potential:

$$\Phi^* = \Phi + \frac{1}{Z_h e} \mu B + \frac{m}{2 Z_h e} \left| \mathbf{v}_E \right|^2, \tag{10}$$

$$\mathbf{A}^* = \mathbf{A} + \frac{m v_{\|}}{Z_h e} \mathbf{b} + \frac{m}{Z_h e} \mathbf{v}_E. \tag{11}$$

It should be noted that the $\mathbf{E}\times\mathbf{B}$ drift velocity ($\mathbf{v}_E = \mathbf{E}\times\mathbf{B}/B^2$) is introduced into $\mathbf{A}^*$ and the polarization drift velocity now appears explicitly in the guiding-center velocity expression (8).

D. Formalism of energetic particles current

The energetic particle current density $\mathbf{J}_h$ consists of three parts : the guiding center current $\mathbf{J}_{\rm GC}$, the magnetization current $\mathbf{J}_{\rm MAG}$, and the polarization current $\mathbf{J}_{\rm POL}$:

$$\mathbf{J}_h = \mathbf{J}_{\rm GC} + \mathbf{J}_{\rm MAG} + \mathbf{J}_{\rm POL}. \tag{12}$$

$\mathbf{J}_{\rm GC}$ is associated with the guiding center drift velocity:

$$\mathbf{J}_{\rm GC} = \int Z_h e(\mathbf{v}_{_{\rm curvature}} + \mathbf{v}_{_{\nabla B}} + \mathbf{v}_B + \mathbf{v}_{EB}) f(\mathbf{X}, v_\parallel, \mu)\delta\left(\mathbf{x} - \mathbf{X} - \boldsymbol{\rho}_h\right) \mathscr{J}_{\rm GC} d\mathbf{X} dv_\parallel d\mu d\alpha, \tag{13}$$

where

$$\mathbf{v}_{_{\rm curvature}} = \frac{m v_\parallel^2}{Z_h e B_\parallel^*}\nabla\times\mathbf{b}, \tag{14}$$

$$\mathbf{v}_{_{\nabla B}} = \frac{\mu}{Z_h e B_\parallel^*}\mathbf{b}\times\nabla B, \tag{15}$$

$$\mathbf{v}_B = v_\parallel \frac{\mathbf{B}}{B_\parallel^*}, \tag{16}$$

$$\mathbf{v}_{EB} = \frac{m}{Z_h e B_\parallel^*}\left[v_\parallel \nabla\times\mathbf{v}_E + \frac{1}{2}\mathbf{b}\times\nabla\left|\mathbf{v}_E\right|^2 + v_\parallel \mathbf{b}\times\frac{\partial\mathbf{b}}{\partial t}\right]. \tag{17}$$

Both linear and nonlinear benchmarks based on the internal kink mode, the tearing mode, and the TAE have been carried out to validate the credibility and applicability of CLT[15] and CLT-K[14]. The detailed descriptions for CLT-K can be found in Ref. [14].

III. SIMULATION RESULTS

A. Basic parameters

In the present simulation, we choose a simple zero beta tokamak equilibrium with shifted circular flux surfaces and a large aspect ratio $R_0/a = 4.0$. The plasma density is assumed to be uniform and the safety factor profile is shown in Figure 1 varying from $q_0 = 1.3$ at the magnetic axis to $q_a = 5.3$ at the edge. The effect of energetic ions on plasma equilibrium

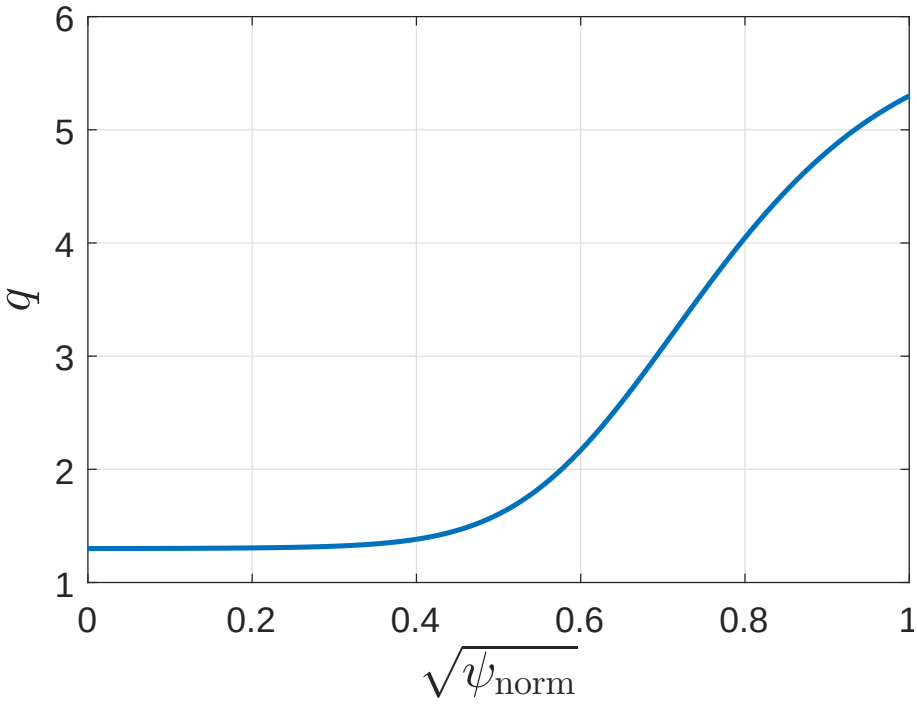

Figure 1: Initial equilibrium profile of the safety profile q

is assumed to be neglected since energetic particle beta β_h is assumed to be small. In the cylindrical coordinate (R, ϕ, Z) of CLT-K, the number of grid points is $128 \times 16 \times 128$ and the viscosity, diffusion, resistivity, and thermal conductivity are set to be $\nu = 1 \times 10^{-5} v_A a$, $D = 1 \times 10^{-6} v_A a$, $\eta = 1 \times 10^{-5} \mu_0 v_A a$, and $\kappa = 1 \times 10^{-6} v_A a$, respectively. The isotropic particle distribution is chosen to be a slowing down distribution in the velocity space and an exponential distribution in the real space,

$$f_0 = \frac{1}{v^3 + v_c^3} \left[1 + \mathrm{erf}\left(\frac{v_0 - v}{\Delta v} \right) \right] \exp\left(-\frac{\langle \psi \rangle}{0.37 \Delta \psi} \right),$$

where $\langle \psi \rangle$ is an averaged poloidal flux over a particle orbit, which labels an effective orbit center with the given constants of motion (P_ϕ, E, μ):

$$\begin{aligned} \langle \psi \rangle &= -P_\phi/(Z_h e) + \frac{m}{Z_h e} \left\langle v_\parallel R \frac{B_\phi}{B} \right\rangle \\ &= \begin{cases} -P_\phi/(Z_h e) & , \ \mu B_0/E > 1 \text{ for trapped particles} \\ -P_\phi/(Z_h e) + \frac{m}{Z_h e} \mathrm{sgn}(v_\parallel) v R_0 \sqrt{1 - \mu B_0/E} & . \ \mu B_0/E \leq 1 \text{ for passing particles} \end{cases} \end{aligned}$$

It should be noted that in the simulation, we retain only the $n = 1$ component of the energetic particle current, and the difference between the single and multiple MHD mode

simulations is whether only the $n = 1$ mode remains in the MHD part.

B. Simulation results

1. Tearing mode from MHD

First, a pure MHD simulation is carried out to validate tearing mode physics. For the giving initial equilibrium, the $m/n = 2/1$ tearing mode is linearly unstable and the scaling law of the linear growth rate is $\gamma \propto \eta^{3/5}$, which agrees well with the analytical result. The toroidal electric field at the linear stage is shown in Figure 2 and the mode structure is localized around the $q = 2$ rational surface as expected. For the nonlinear stage, it is interestingly to find in Figure 3 that the tearing mode with a single toroidal mode number is not saturated. As we know, the $m/n = 2/1$ tearing mode is unstable only around the $q = m/n = 2$ rational surface. Thus, if the single toroidal mode, $n = 1$, retains, only the $m = 2$ poloidal mode is left, which leads to that both toroidal and poloidal mode couplings are missed. As shown in Figure 3, the zonal component , $n = 0$, is even much crucial for the tearing mode nonlinear saturation, especially for a beating part generated by two single tearing modes themselves, which suggests that the mode-mode coupling is important for the nonlinear saturation.

2. Energetic particle effects on Tearing mode

Energetic particle effects on the tearing mode are studied by using hybrid simulation. First, we examine the role of energetic particle beta on tearing mode dynamics with the fixed resistivity $\eta = 1 \times 10^{-5}$. It is found in Figure 4 that for the small β_h cases (β_h∼0.004-0.006), the tearing mode is stabilized weakly by energetic particles at the linear stage, which is quite similar to previous simulation results from the NIMROD code[11]. For the large β_h cases, a TAE excited by energetic particles becomes the dominant unstable mode because the growth rate of the TAE is much larger than that of the $m/n = 2/1$ tearing mode. For nonlinear stage, it is found that the TAE will be saturated before the tearing mode plays a role for the large β_h cases (β_h\sim0.008 and 0.010) and the final saturation level is enhanced with increase of β_h. To understand dynamic process during the period of coexistence of

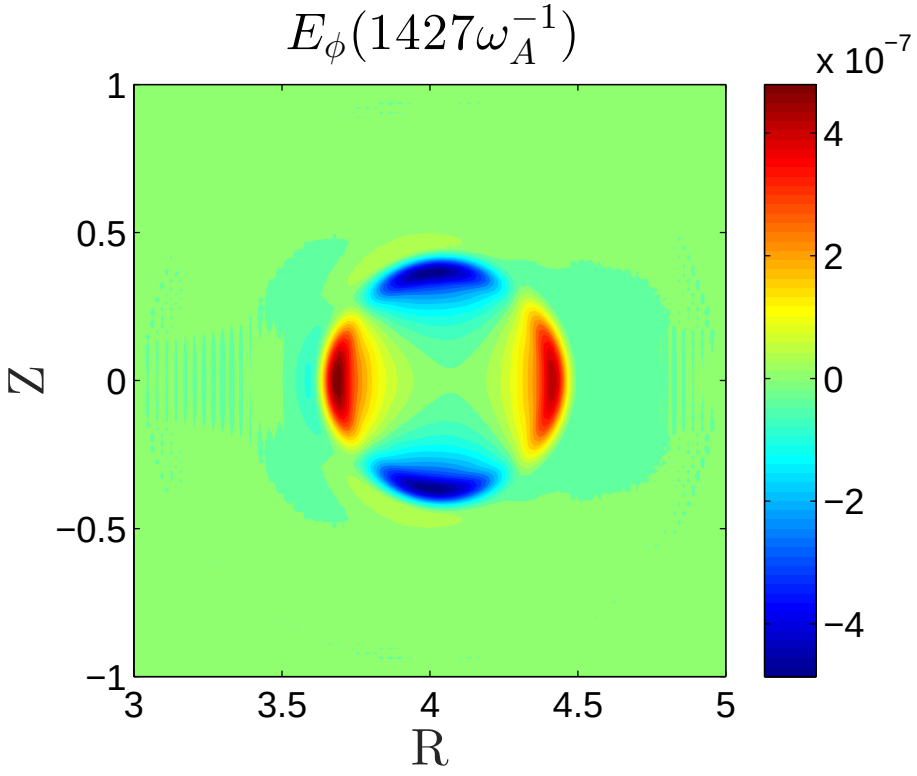

Figure 2: Contour plot of toroidal electric field for the $m/n = 2/1$ tearing mode

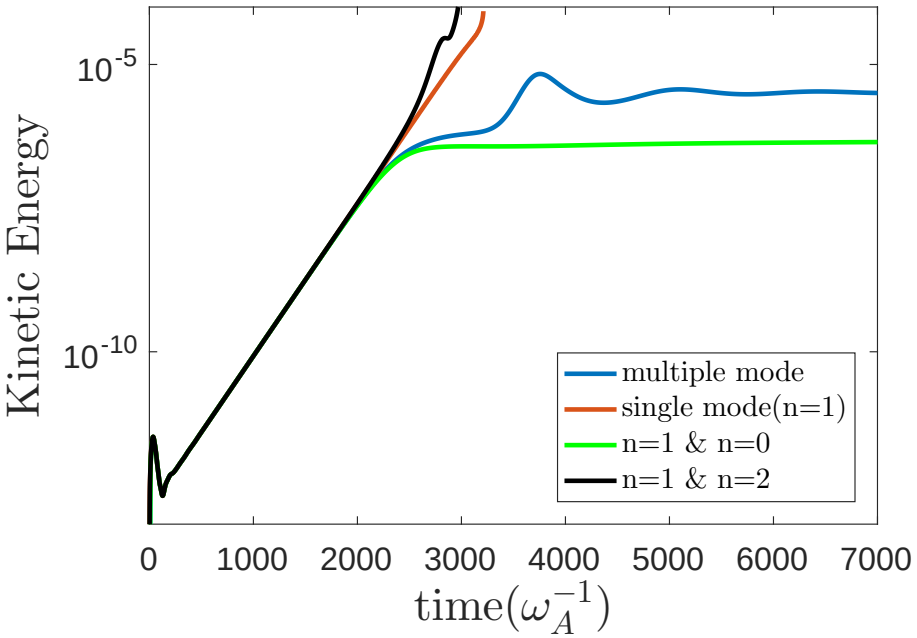

Figure 3: Time evolutions of the kinetic energy from single and multiple mode simulations.

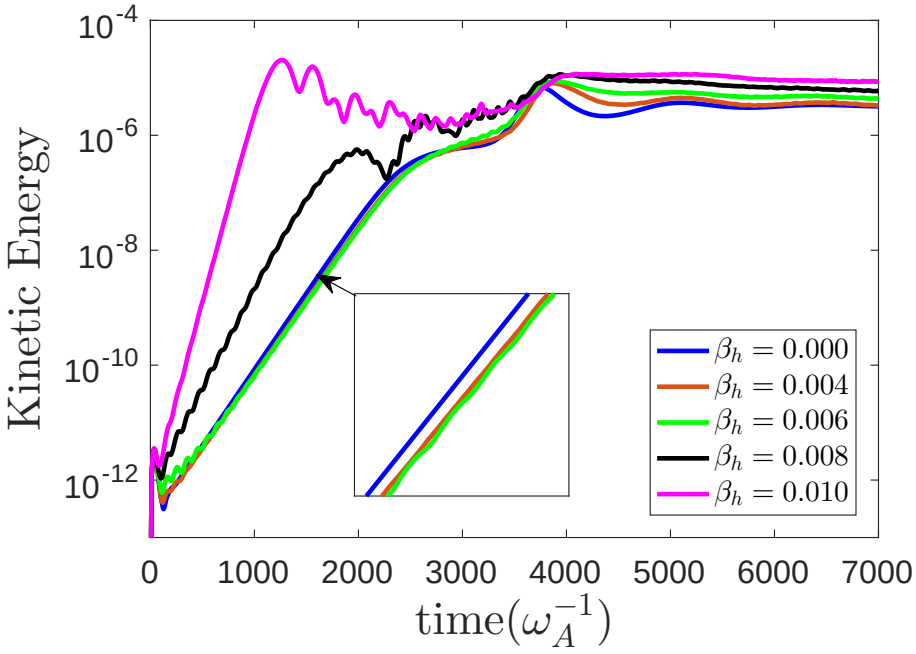

Figure 4: Time evolutions of the kinetic energy for different β_h.

TAEs and tearing modes, we further examine the $\beta_h = 0.008$ case in detail.

Figure 5 shows time evolutions of the kinetic energy for the single $n = 1$ and multiple MHD mode simulations. As mentioned before, the tearing mode in the single mode simulation is not saturated due to lack of nonlinear MHD mode couplings. Thus, the first saturation of the TAE should be resulted from wave-particle interactions. For the multiple mode simulation, there are extra two saturation states due to mode-mode coupling or wave-wave interaction. Figure 6 shows the mode structures of the toroidal electric field at three different stages. In the early linear stage ($t \sim 1784\omega_A^{-1}$), the toroidal electric field indicates that there are two dominant poloidal harmonics (m and $m + 1$), which strongly suggests that the dominant mode is a TAE mode. After the first saturation, the continuous growth of the $m/n = 2/1$ tearing mode becomes dominant. As shown in Figure 6(b), the mode structure of the toroidal electric field shows a typical tearing mode structure. At the late nonlinear stage ($t \sim 4636\omega_A^{-1}$), the $m/n = 6/3$ and $3/2$ modes become comparable with the $m/n = 2/1$ harmonics. Therefore, we can conclude from the evolution of the mode structures that the second saturation is resulted from the interaction between the primary $2/1$ tearing mode and the zonal component and the third saturation is caused by multiple tearing mode interaction.

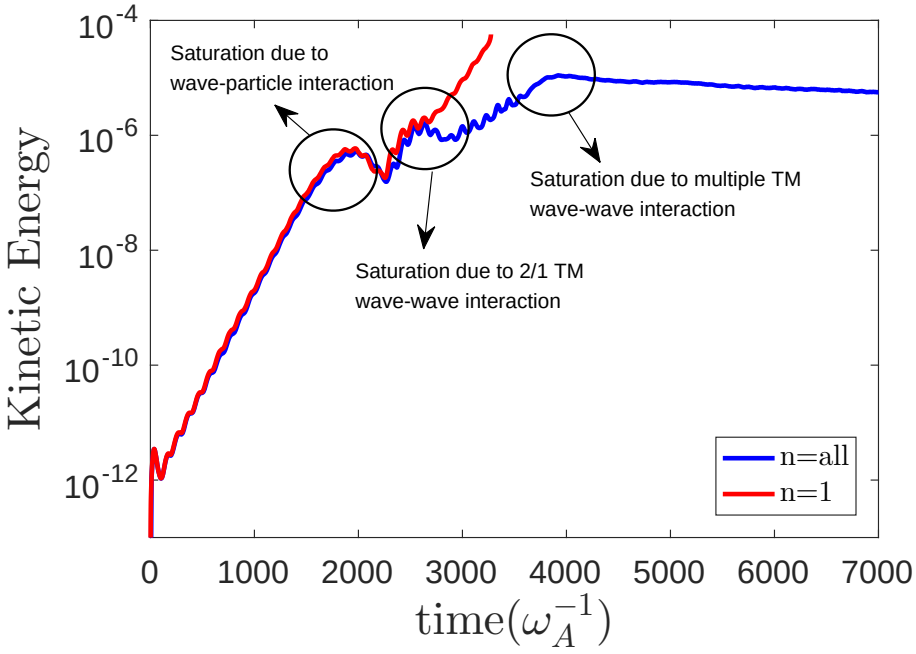

Figure 5: Time evolutions of the total kinetic energy from single and multiple MHD mode simulations for $\beta_h = 0.008$

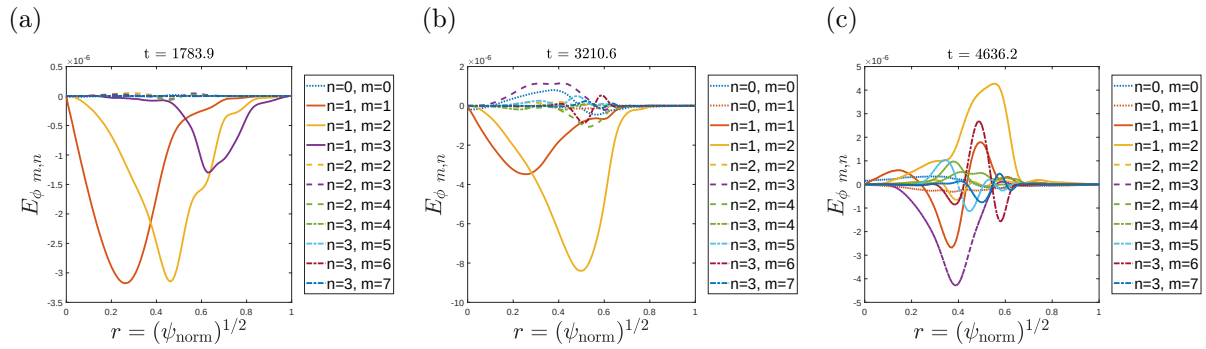

Figure 6: Toroidal components of the electric field at three different stages

It is also interested that an oscillatory growth of the kinetic energy is observed. Because there are the two eigenmode modes (TAE and tearing mode) in the system, the superposition of these two unstable modes causes the oscillatory growth of the kinetic energy. The similar phenomena of the oscillatory growth induced by superposition of the two eigenmodes were also reported in the double-resonant fast particle-wave interaction from a reduced model[18] and the double tearing mode evolution in the presence of shear flows from the reduced resistive MHD model in a slab geometry[19].

The time evolutions of the frequency spectrum for the primary $n = 1$ mode and the

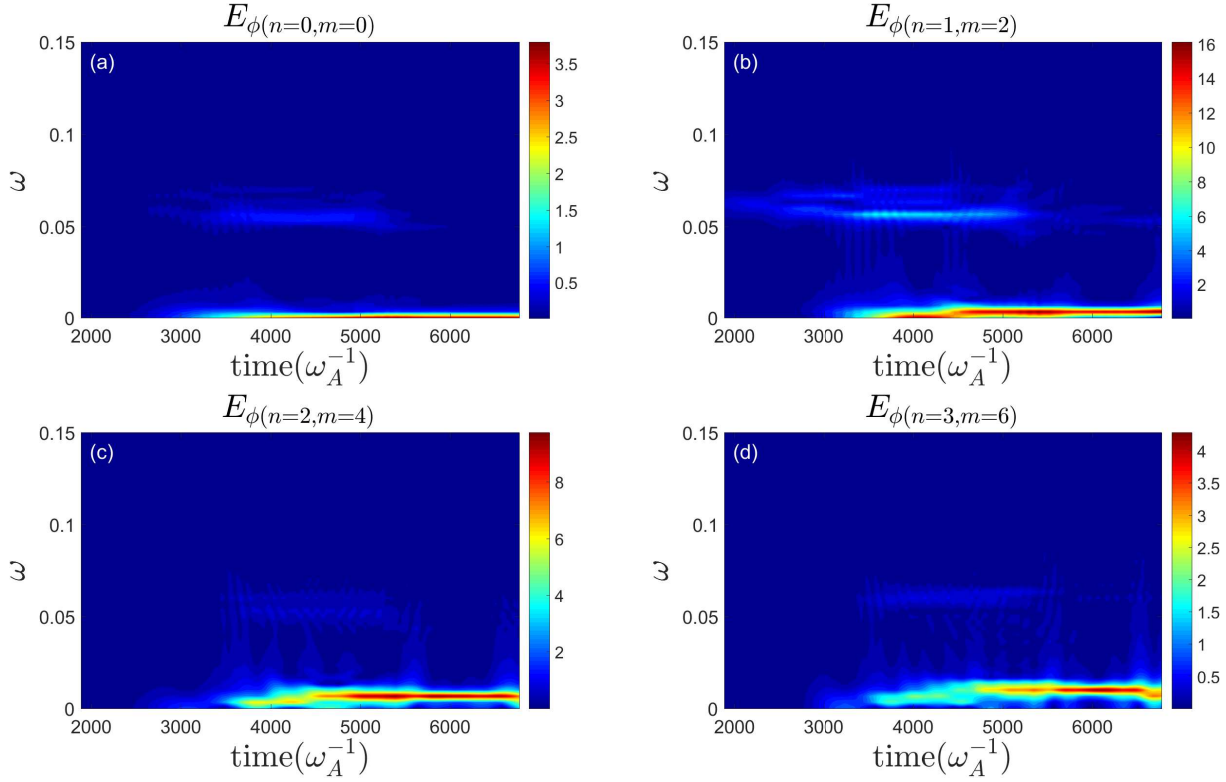

Figure 7: Time evolutions of the frequency spectrum for different toroidal modes

sideband modes are shown in Figure 7. It is indicated that all signals with different toroidal modes have two branches in the late stage: the high frequency branch (TAE) and the low frequency branch (Tearing Mode). For the primary mode ($n = 1, m = 2$), the signal of the TAE is strong at the early nonlinear phase when wave-particle interaction is dominant. The signal of the tearing mode starts to become much stronger at $t = 3500\omega_A^{-1}$, which is corresponding to the second saturation stage due to wave-wave interaction.

As shown in Figure 8(b), the linear growth rates of two side-band modes ($n = 0$ and $n = 2$) of the $n = 1$ mode are about double of the dominant $n = 1$ mode, which suggests that $n = 0$ and $n = 2$ modes are primarily resulted from the coupling of the two $n = 1$ harmonics of the TAE mode. This phenomenon is also observed by another hybrid simulation from the MEGA code [20]. At the nonlinear stage, the $n = 0$ mode has the higher saturation level than that from the MHD simulation, which means that the higher linear growth rate of the zonal flow or the stronger coupling of the two $n = 1$ energetic particle current J_h could lead to the enhancement of the $n = 0$ nonlinear saturation level.

It is well known that both tearing mode and TAE are electromagnetic perturbations,

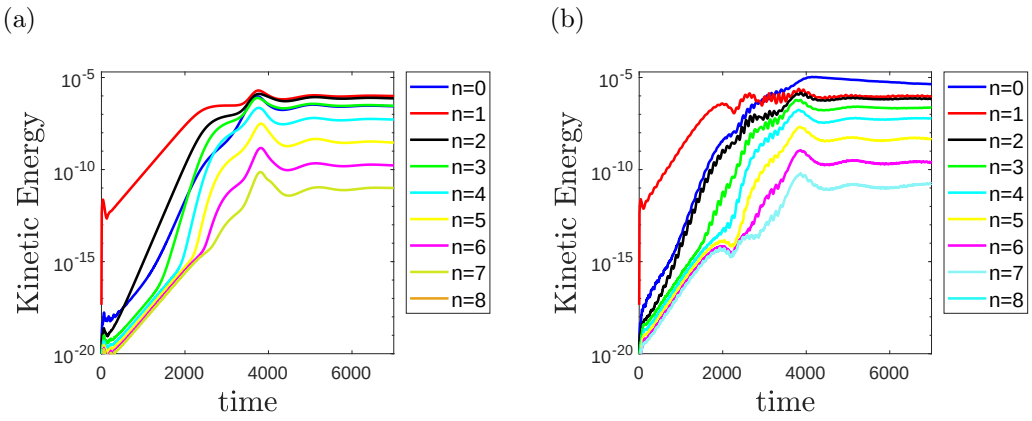

Figure 8: Comparisons for evolution of kinetic energy w/o energetic particles

which leads to difficulty to distinguish them from the mode structures. But, from radial structures of the mode frequency [14], we are able to distinguish the TAE and the tearing mode. In Figure 9(a)-(d), we show radial structures of the mode frequency measured at the midplane ($\theta = 0$) of the weak field side. The modes are only one frequency around $\omega = 0.06\omega_A^{-1}$ in the early stage in Figure 9(a), which is corresponding to the high frequency TAE excited by EP at the linear phase. It is interestingly found that at $t = 2480\omega_A^{-1}$, the mode frequency starts to split in the region outside $\sqrt{\psi_{\rm norm}}$ ~0.4 while the frequency in the region inside it remains unchanged. Through carefully examining different poloidal components of the mode, especially for m/n=1/1 and 2/1, it is noticed that the m/n=2/1 component splits first into two branches in Figure 9(j) while the m/n=1/1 component remains the single branch at $t = 2480\omega_A$ in Figure 9(f), which is coincident with that the amplitude of the low frequency tearing mode reaches to a comparable level related to the TAE as shown in Figure 9(b). It is suggested that the frequency splitting of the TAE is associated with the strong tearing mode activities. In the linear phase, the $m/n = 1/1$ and $m/n = 2/1$ poloidal harmonics of the TAE can be considered as two "degenerated" states that share the same TAE frequency, but dynamics of these two poloidal harmonics can be decoupled due to the nonlinear effect.

3. Resistivity effect on frequency chirping of TAE

Since a tearing mode instability affects the frequency splitting of the TAE, it is worthwhile to investigate the tearing mode effect on dynamic of the $n = 1$ TAE with different resistivities

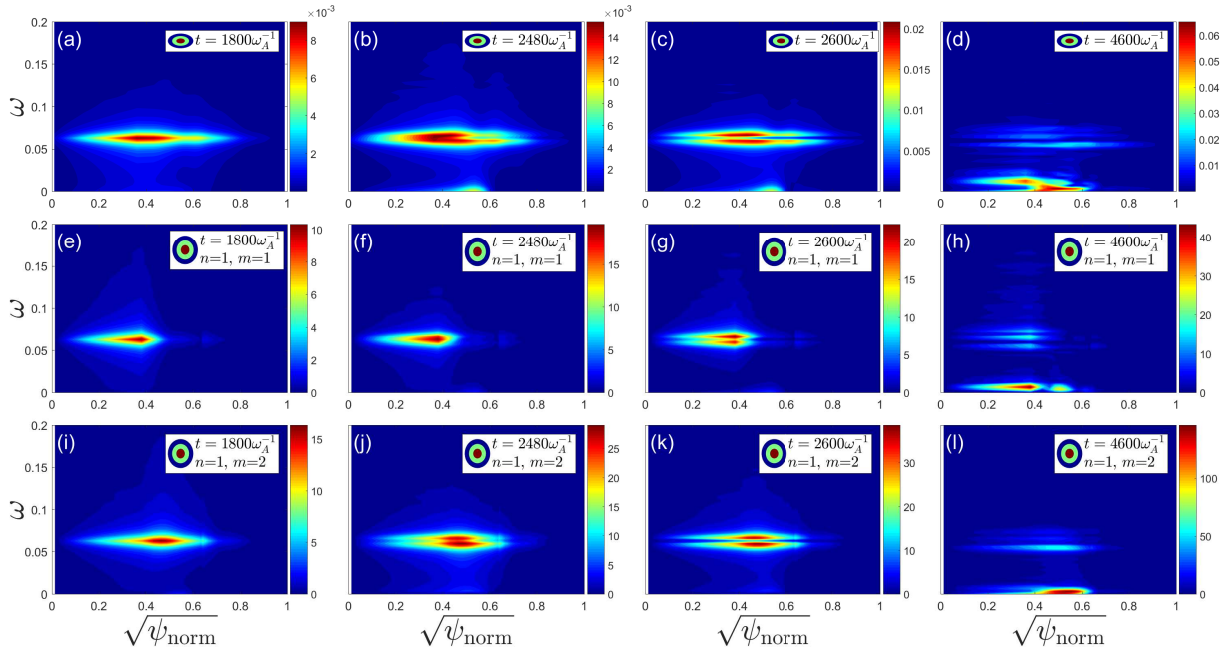

Figure 9: Radial structures of the mode frequency at different times

η. It should be noted that a larger viscosity ($\nu = 2 \times 10^{-5}$) is used to control numerical stability for cases with a small resistivity. The range of the resistivity is chosen to be from 1×10^{-7} to 5×10^{-5}. The results as shown in Figure 10 indicate that the resistivity plays a damping role on TAE for the resistivity $\eta < 2 \times 10^{-5}$. For the large resistivity $\eta \geq 5 \times 10^{-5}$, the growth rate of the tearing mode becomes larger than that of TAE. Thus, the tearing mode becomes dominant.

For the nonlinear stage, the results in Figure 11 suggest that for cases with small resistivity, the nonlinear saturation is only govern by wave-particle interactions and the mode evolution exhibits a nonlinear oscillation that is similar with that in previous TAE simulations [21, 22]. For cases with moderate resistivity, the nonlinear dynamics is controlled by both the TAE and the tearing mode. For cases with large resistivity, the nonlinear saturation is due to mode-mode coupling since the tearing mode is dominant.

Nonlinear TAE frequency chirping is also examined with different resistivities. Figure. 12 shows three cases with: (a)small resistivity $\eta = 10^{-7}$, (b)moderate resistivity $\eta = 10^{-5}$, and (c)large resistivity $\eta = 2 \times 10^{-5}$. Since we are only interested in the TAE activity, we just choose the frequency range from 0.03 to 0.14 to hide the strong tearing mode activities. It is interestingly found that, for the small resistivity, the frequency chirping shows up-down symmetry structure which is consistent with previous TAE simulation results[21, 23], while

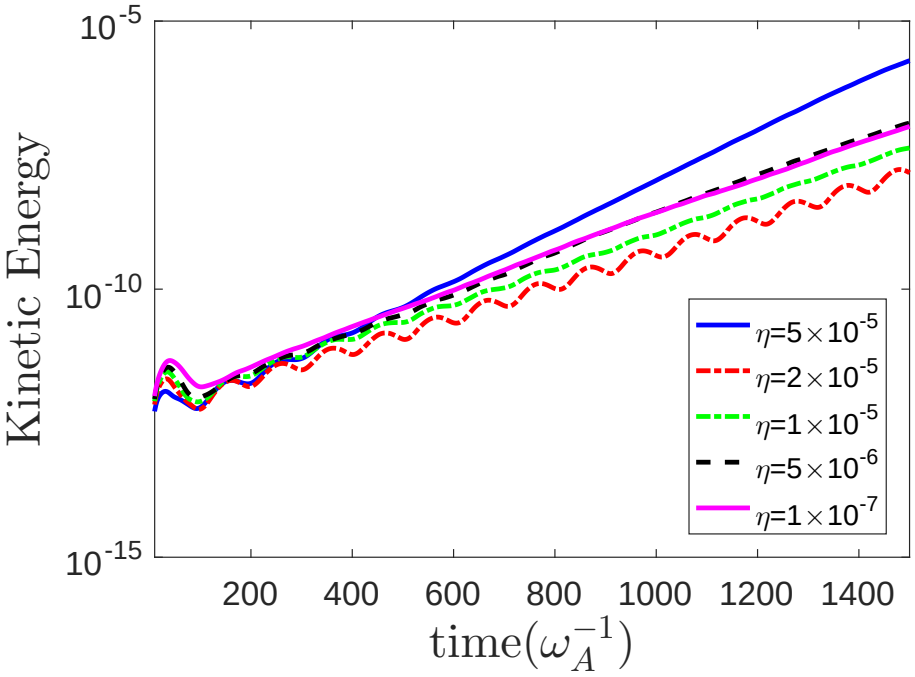

Figure 10: Time evolutions of the kinetic energy with different resistivities in the linear stage

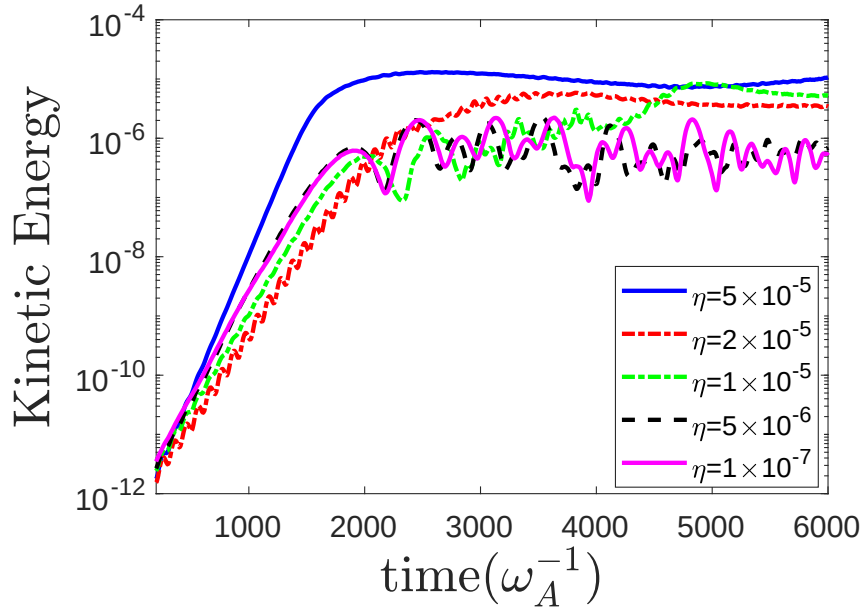

Figure 11: Time evolutions of the kinetic energy with different resistivities at the nonlinear stage

the frequency chirping phenomenon becomes weaker due to strong tearing mode activity in cases with large resistivity. This simulation result is also consistent with experiment results on HL-2A that show no frequency chirping of TAE modes in the presence of strong low

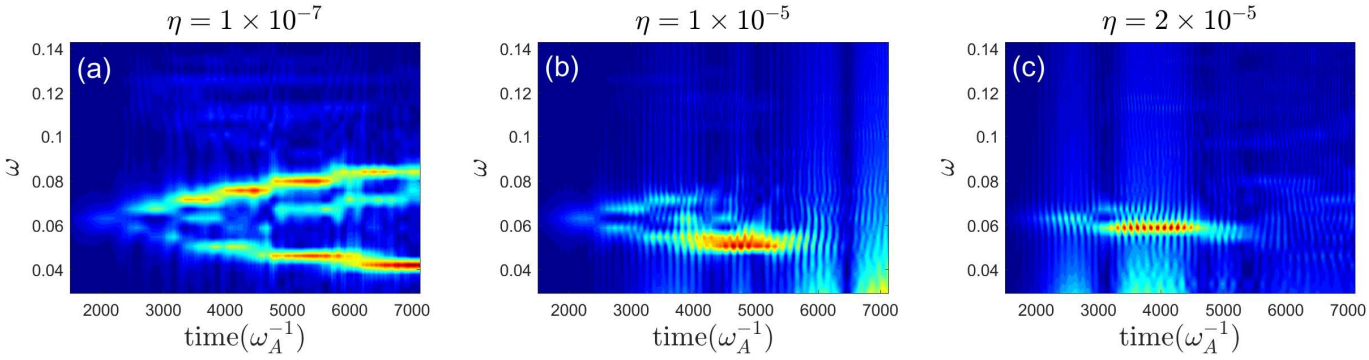

Figure 12: Time evolution of the TAE mode frequency with different resistivities

frequency tearing modes[4, 5]. It should be pointed out that the required marginal growth rate of TAE for the frequency chirping in the classical picture is $\gamma_L - \gamma_d \ll \gamma_L$. Increase of the dissipation (such as the resistivity, the viscosity) leads to the system closer to the marginal state, and then a frequency chirping of TAE occurs, which can be found in theoretical work based on Berk-Breizman model[24, 25] and numerical work based on reduced model[21, 22]. The simulation results reported here suggest that the resistive dissipation plays an opposite role on the TAE frequency chirping, i.e., the enhancement of the tearing mode activity due to increase of the resistivity leads to weaken the frequency chirping of the TAE mode.

In order to further clarify the effect of tearing modes on TAE frequency chirping, we plot the δf structure in the $(E, \langle\psi\rangle)$ phase space, where $\langle\psi\rangle$ is an averaged poloidal flux that is the function of the three constant motions:E, P_ϕ, and Λ. Compared with canonical angular momentum P_ϕ, $\langle\psi\rangle$ is more intuitive to be identified as a radial function. It is found in Figure 13 that for a weak tearing mode activity, the δf structure in the phase space shows hole-clump pair generation in the early stage and then expansion associated with the TAE frequency up-down symmetric chirping in the nonlinear phase. The phenomenon of the pitch-fork frequency chirping without tearing modes is consistent with previous simulation result based on the reduced model[21, 22] and the hybrid model[23]. For the moderate resistivity ($\eta = 10^{-5}$), the effect of tearing modes on the TAE frequency chirping becomes more significant, which can be found in Figure 14. In the linear phase, the $p = 1$ poloidal resonance associated with the TAE is dominant as shown in Figure 14(a). After the saturation of the tearing mode, the $p = 2$ poloidal resonance associated with the low frequency tearing mode becomes evident in the low energy region and the q=2 surface ($\langle\psi\rangle \sim -0.11$) as shown in Figure. 14(b). At the late nonlinear stage, the "local" $p = 2$ resonance related to the

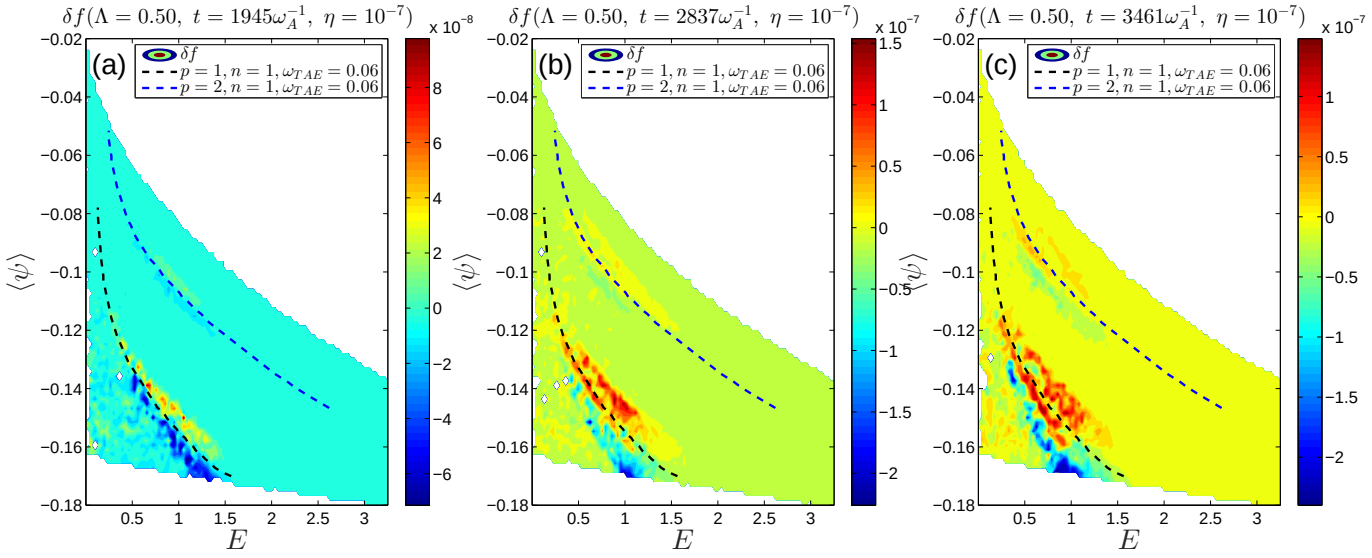

Figure 13: δf structures at different times for a small resistivity $\eta = 10^{-7}$ with $\Lambda = 0.5$

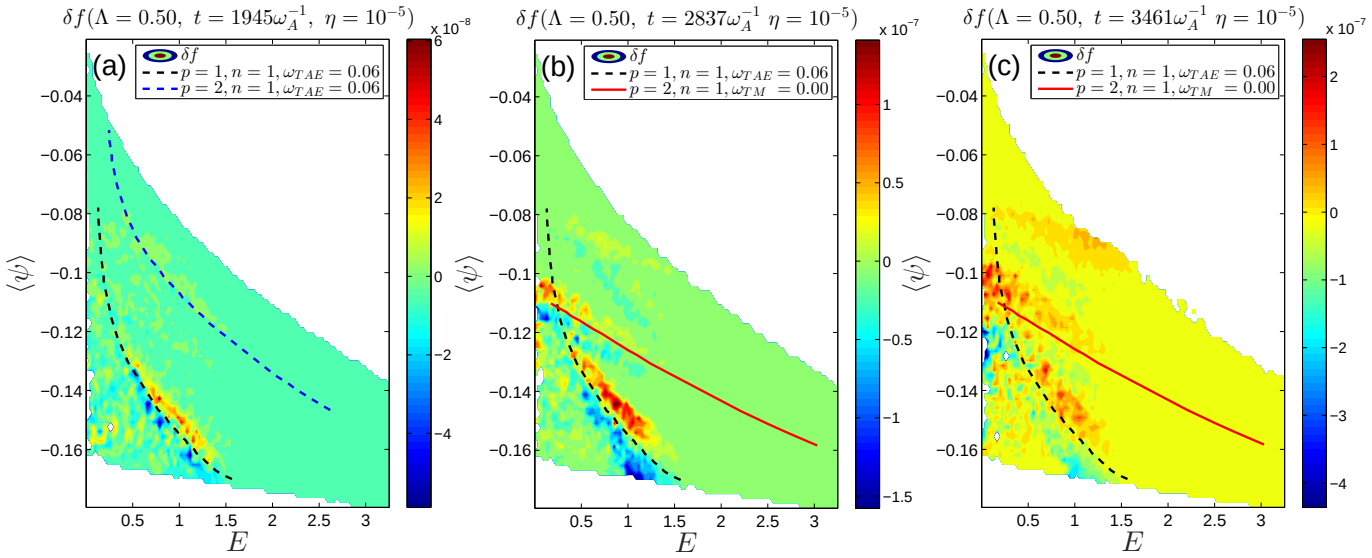

Figure 14: δf structures at different times for a moderate resistivity $\eta = 10^{-5}$ with $\Lambda = 0.5$

tearing mode becomes broad and affect the expansion of the $p = 1$ poloidal resonance of the TAE. Similar phenomena in the phase space are also observed for the small Λ cases (such as $\Lambda = 0.00, 0.25$), but it is more evident for the case with $\Lambda = 0.50$.

Resonance structures for trapped particles in the phase space are also presented in Figure 15. It is found that the locations between the tearing mode and TAE are far away, thus the interaction between the tearing mode and TAE is weak for trapped particle resonances.

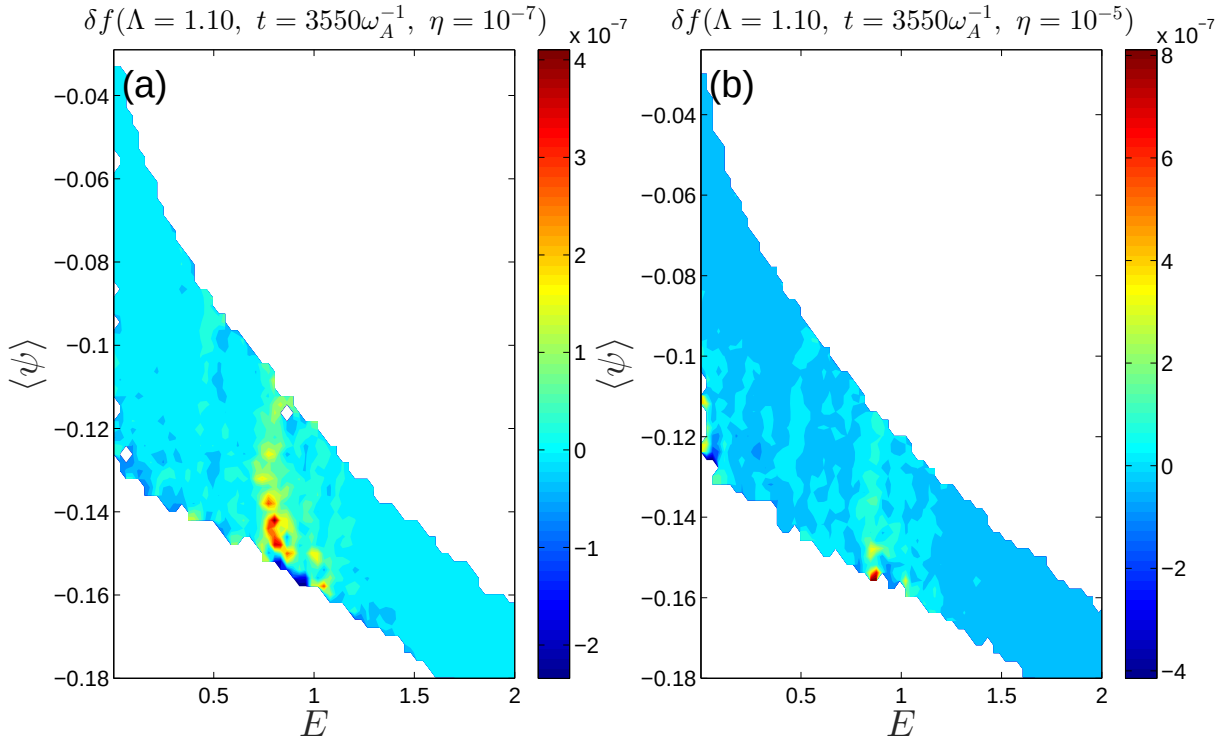

Figure 15: δf structures for different resistivities with $\Lambda = 1.1$

IV. CONCLUSION

The hybrid simulations are carried out to investigate nonlinear dynamics of the TAE in the presence of the tearing mode. It is found that the saturation of the TAE is due to wave-particle interaction and the saturation of the tearing modes is resulted from the mode-mode coupling. The frequency spectrum shows both the high frequency TAE branch and the low frequency tearing mode branch, which is very similar with experimental observations in HL-2A and J-TEXT. It is interestingly found that the role of the resistive dissipation on the frequency chirping is opposite to that in the classical physical picture, in which increase of dissipations leads to the system closer to a marginal state ($\gamma_L - \gamma_d \ll \gamma_L$) of significant frequency chirping. In the present results, it is suggested that the strong tearing mode activity associated with large resistivity could weaken the TAE frequency chirping through the interaction between the $p = 1$ TAE resonance and the $p = 2$ tearing mode resonance for passing particles in the phase space. Therefore, the resistivity plays an important role in the TAE frequency chirping.

Acknowledgments

We would like to thank Professor Guo-Yong Fu for his useful suggestions. One of the authors (Jia Zhu) gratefully thanks Peiwan Shi for many valuable discussions. This work was funded by Fundamental Research Fund for Chinese Central Universities, National Magnetic Confinement Fusion Science Program of China under Grant No. 2013GB104004 and 2013GB111004, the Special Project on High-performance Computing under the National Key R&D Program of China No. 2016YFB0200603, China Postdoctoral Science Foundation under Grant No. 2015M571859, the National Natural Science Foundation of China under Grant No. 41474123 and 11505152.

---

[1] N. N. Gorelenkov, S. D. Pinches, and K. Toi. Energetic particle physics in fusion research in preparation for burning plasma experiments. *Nuclear Fusion*, 54(12):125001, 2014.

[2] C. Z. Cheng, Liu Chen, and M. S. Chance. High-n ideal and resistive shear alfvén waves in tokamaks. *Annals of Physics*, 161(1):21–47, 1985.

[3] C. Z. Cheng and M. S. Chance. Low-n shear alfven spectra in axisymmetric toroidal plasmas. *Physics of Fluids*, 29(11):3695, 1986.

[4] W. Chen, Z. Qiu, X. T. Ding, H. S. Xie, L. M. Yu, X. Q. Ji, J. X. Li, Y. G. Li, J. Q. Dong, Z. B. Shi, Y. P. Zhang, J. Y. Cao, X. M. Song, S. D. Song, M. Xu, Q. W. Yang, Yi Liu, L. W. Yan, and X. R. Duan. Observation and theory of nonlinear mode couplings between shear alfvén wave and magnetic island in tokamak plasmas. *EPL (Europhysics Letters)*, 107(2):25001, 2014.

[5] P. W. Shi, W. Chen, Z. B. Shi, X. R. Duan, L. M. Yu, W. L. Zhong, M. Jiang, Z. C. Yang, J. X. Li, J. Wen, X. T. Ding, Yi. Liu, and Q. W. Yang. Destabilization of toroidal alfvén eigenmode during neutral beam injection heating on hl-2a. *Physics of Plasmas*, 24(4):042509, 2017.

[6] Wei Chen, Min Jiang, Yuhong Xu, Peiwang Shi, Liming Yu, Xuantong Ding, Zhongbing Shi, Xia Quan Ji, Deliang Yu, Yonggao Li, Zengchen Yang, Wulyu Zhong, Zhiyong Qiu, Jiquan Li, Jiaqi Dong, Qingwei Yang, Yi Liu, Longwen Yan, Min Xu, and Xuru Duan. Experimental observation of multi-scale interactions among kink/tearing modes and high-frequency fluctuations in the hl-2a core nbi plasmas. *Nuclear Fusion*, 2017.

[7] Linzi Liu, Jiyang He, Qiming Hu, and Ge Zhuang. Observation of beta-induced alfvén eigenmode in j-text tokamak. *Plasma Physics and Controlled Fusion*, 57(6):065007, 2015.

[8] G. Y. Fu, W. Park, H. R. Strauss, J. Breslau, J. Chen, S. Jardin, and L. E. Sugiyama. Global hybrid simulations of energetic particle effects on the n=1 mode in tokamaks: Internal kink and fishbone instability. *Physics of Plasmas*, 13(5):052517, 2006.

[9] Liu Chen. *Theory of Fusion Plasmas(Bologna: Editrice Compositori) ed J. Vaclavik, F. Troyon and E. Sindoni*, pages 327–388, 1988.

[10] G. Y. Fu and J. W. Van Dam. Excitation of the toroidicity-induced shear alfven eigenmode by fusion alpha particles in an ignited tokamak. *Physics of Fluids B: Plasma Physics*, 1(10):1949, 1989.

[11] R. Takahashi, D. P. Brennan, and C. C. Kim. Kinetic effects of energetic particles on resistive mhd stability. *Physical Review Letters*, 102(13), 2009.

[12] H. Cai, S. Wang, Y. Xu, J. Cao, and D. Li. Influence of energetic ions on tearing modes. *Phys Rev Lett*, 106(7):075002, 2011.

[13] Huishan Cai and Guoyong Fu. Hybrid simulation of energetic particle effects on tearing modes in tokamak plasmas. *Physics of Plasmas*, 19(7):072506, 2012.

[14] J. Zhu, Z. W. Ma, and S. Wang. Hybrid simulations of alfvén modes driven by energetic particles. *Physics of Plasmas*, 23(12):122506, 2016.

[15] S. Wang and Z. W. Ma. Influence of toroidal rotation on resistive tearing modes in tokamaks. *Physics of Plasmas*, 22(12):122504, 2015.

[16] W. Park, S. Parker, H. Biglari, M. Chance, L. Chen, C. Z. Cheng, T. S. Hahm, W. W. Lee, R. Kulsrud, D. Monticello, L. Sugiyama, and R. White. Three-dimensional hybrid gyrokinetic-magnetohydrodynamics simulation. *Physics of Fluids B: Plasma Physics*, 4(7):2033, 1992.

[17] John R. Cary and Alain J. Brizard. Hamiltonian theory of guiding-center motion. *Reviews of Modern Physics*, 81(2):693–738, 2009.

[18] M. Schneller, Ph Lauber, M. Brüdgam, S. D. Pinches, and S. Günter. Double-resonant fast particle-wave interaction. *Nuclear Fusion*, 52(10):103019, 2012.

[19] Aohua Mao, Jiquan Li, Y. Kishimoto, and Jinyuan Liu. Eigenmode characteristics of the double tearing mode in the presence of shear flows. *Physics of Plasmas*, 20(2):022114, 2013.

[20] Y. Todo, H. L. Berk, and B. N. Breizman. Nonlinear magnetohydrodynamic effects on alfvén eigenmode evolution and zonal flow generation. *Nuclear Fusion*, 50(8):084016, 2010.

[21] J. Zhu, G. Y. Fu, and Z. W. Ma. Nonlinear dynamics of toroidal alfvet'n eigenmodes driven by energetic particles. *Physics of Plasmas*, 20(7):072508, 2013.

[22] S. D. Pinches, H. L. Berk, M. P. Gryaznevich, S. E. Sharapov, and Jet-Efda Contributors. Spectroscopic determination of the internal amplitude of frequency sweeping tae. *Plasma Physics and Controlled Fusion*, 46(7):S47–S57, 2004.

[23] Jianying Lang, Guo-Yong Fu, and Yang Chen. Nonlinear simulation of toroidal alfven eigenmode with source and sink. *Physics of Plasmas*, 17(4):042309, 2010.

[24] H. L. Berk, B. N. Breizman, and M. Pekker. Nonlinear dynamics of a driven mode near marginal stability. *Physical Review Letters*, 76(8):1256–1259, 1996.

[25] H. L. Berk, B. N. Breizman, and N. V. Petviashvili. Spontaneous hole-clump pair creation in weakly unstable plasmas. *Physics Letters A*, 234(3):213–218, 1997.